PERGAMON

Corrosion Science 42 (2000) 1881–1895

CORROSION SCIENCE

www.elsevier.com/locate/corsci

Influence of sputtering conditions on corrosion of sputtered W–Ti–N thin film hard coatings: salt spray tests and image analysis

João Carlos Oliveira[a], Albano Cavaleiro[a], Christopher M.A. Brett[b,*]

[a]*Departmento de Engenharia Mecânica, ICEMS, Faculdade de Ciências e Tecnologia, Universidade de Coimbra 3049 Coimbra, Portugal*

[b]*Departamento de Química, ICEMS, Faculdade de Ciências e Tecnologia, Universidade de Coimbra, 3049 Coimbra, Portugal*

Received 16 June 1999; accepted 7 March 2000

Abstract

The corrosion resistance of sputter-coated W–Ti–N films on high speed steel substrates prepared under different deposition conditions has been compared by varying the film surface roughness, the film thickness and depositing a first W–Ti layer. Salt spray tests have been carried out and the resulting pitting corrosion evaluated by image analysis and by microscopy and X-ray diffraction. The results show that the most important factors influencing corrosion are film compactness and thickness. The detailed mechanism of corrosion is discussed, involving electrolyte penetration with substrate corrosion, the corrosion products either blocking further corrosion or leading to localised film rupture. © 2000 Elsevier Science Ltd. All rights reserved.

Keywords: Sputtered hard coatings; W-based coatings; Corrosion; Salt spray test; Image analysis

* Corresponding author. Fax: +351-39-835295.
E-mail address: brett@ci.uc.pt (C.M.A. Brett).

0010-938X/00/$ - see front matter © 2000 Elsevier Science Ltd. All rights reserved.
PII: S0010-938X(00)00041-X

1. Introduction

Pitting corrosion can occur in sputtered hard coatings in aqueous chloride media, with pits appearing at microscopic flaws in the films. Previous work has demonstrated that this is the case for a number of different types of coatings based on the W–Ti–N and W–Ni–N systems [1,2]. A model was proposed for the appearance of pits which is in accordance with visual and electrochemical observations and involves bubble formation followed by cracking of the coating and corrosion of the high-speed steel substrate [3]. Additionally, it was found that the saline environment does not affect the hardness of the coatings except in the localised zones where corrosion of the substrate has occurred [4].

A further factor which may influence the extent of pitting corrosion is the film morphology, due to its effect on the ease of electrolyte penetration through the substrate. This in turn may be affected by the conditions during sample preparation and the sputtering deposition process itself, in particular the surface roughness of the substrate resulting from ion-etch cleaning of the substrate within the sputtering chamber, carried out to improve coating adhesion. If etching conditions are made more aggressive (increasing etching time, ion current or ion energy) the surface roughness increases, so that a good compromise between efficient cleaning of the surface and surface roughness must be reached. This, as well as the microstructure [5], can influence the corrosion resistance.

Studies have been made in the past regarding the nucleation of pits and their distribution over sample surfaces. In particular, a spectrum of induction periods suggests different susceptibilities at different types of sites on the metal surface [6,7]. Stochastic models for pit initiation and growth on stainless steels have been developed at constant potential [8–10], parameters including transition from unstable to stable pits, i.e. when the pit exceeds a critical depth the value of which is related to the surface roughness, and the death probability of unstable pits [9,10].

A more recent study used image analysis to investigate correlations between human perception of corrosion level (often used in practice) and passivity breakdown [11]. A large number of rusted stainless steel panels were classified according to their perceived dirtiness and found that this corresponded well to the degree of passivity breakdown via a 2-D plot, divided into zones, of 'spot' density (i.e. number of rusted areas per unit area of panel) vs. ratio of rusted to non-rusted area divided into zones. Three stages of corrosion were identified which could be correlated with movement on the 2-D plot: firstly, there is an increase in the number of pits with exposure time, secondly, an increase of the area covered by corrosion products and thirdly, expansion of the pits until merging occurs.

In this work, a systematic study of W–Ti–N films prepared under various different deposition conditions has been carried out. Several parameters have been varied to investigate the influence of film morphology. These are: film thickness; different film surface roughness; deposition with a W–Ti film-substrate underlayer and two-layer deposits by interruption of the deposition process halfway through with cleaning of the surface before continuing the deposition. Corrosion has been

carried out in salt spray test chambers and the samples analysed by surface analysis techniques. The number and size distribution of pits has also been analysed and some considerations similar to those described in [11] taken into account. To our knowledge, this is the first time that image analysis has been employed in a study of sputter-coated steels.

2. Experimental

Samples were prepared by reactive magnetron sputtering from a W + 20 wt%Ti target in a Hartec sputtering apparatus; the total pressure was 0.30 Pa, the nitrogen partial pressure being 0.075 Pa.

The substrates were ion-cleaned using an ion gun before deposition. The normal cleaning procedure involves heating by electron bombardment up to temperatures close to 450°C followed by Ar^+ bombardment at increasing negative substrate bias from 0 to 120 V, with 15 s at each bias value in steps of 10 V. Discs of quenched and tempered M2 (AISI) high speed steel, 35 and 12 mm diameter, were used as substrate after polishing with diamond paste down to 1 μm particle size. Specific deposition conditions are detailed in Table 1, Type 1 serving as reference procedure.

The samples were coated on both faces by rotating the sample holder during deposition, and were then subjected to corrosion by salt spray tests, simulating a marine environment, in a Uniclima CNS-100 chamber at 35°C for up to 5 days with a 5% sodium chloride solution injected at 1 bar pressure. Uncoated edge areas were protected with epoxy resin and samples were suspended vertically within the chamber by a thin nylon thread from a tiny hole near the top edge. It was decided that samples would be removed from the test chamber before the end of the test period only if their surface was more than approximately 60% covered with corrosion products. In one case, Type 4, the sample had to be removed after 3 days. All the other corroded samples were removed after 5 days.

Samples were examined by scanning electron microscopy (SEM), before and after being subjected to corrosion tests, in a Jeol T330 Scanning Electron Microscope with a Tracor Northern Microanalysis Accessory (Energy Dispersive X-Ray Spectrometry — EDXS) and by X-ray diffraction (XRD) in a Siemens X-Pert instrument.

Image analysis from photographs of the corrosion pits was done in the following way. Each face of each sample was divided into six equal parts and digitalised images (with a 10 × magnification) were acquired. Each was then analysed visually in order to identify corrosion pits and to paint each pit with a predefined colour using an image editor computer program. As an example, Fig. 1 shows the same image before and after the editing process. This procedure was used since direct image analysis of the digitalised images was not possible due to the non-uniform shape of the corrosion pits. Finally, each image was processed using image analysis software in order to determine the corrosion pit size distribution and the total corroded area.

Table 1
Sputtering deposition parameters for the various W–Ti–N coatings

	Cleaning by Ar^+ bombardment	Deposition	Film thickness (μm)
Type 1	0→ − 120 V, steps of 10 V, 15 s each step	30 min W–Ti–N	3.5
Type 2	As Type 1, but 3 min at −120 V	As Type 1	3.5
Type 3	As Type 1	10 min W–Ti (no N_2 in chamber); 20 min W–Ti–N	3.8
Type 4	As Type 1	15 min W–Ti–N; 15 min wait and surface cleaning; 15 min W–Ti–N	3.2
Type 5	As Type 1	60 min W–Ti–N	7.5

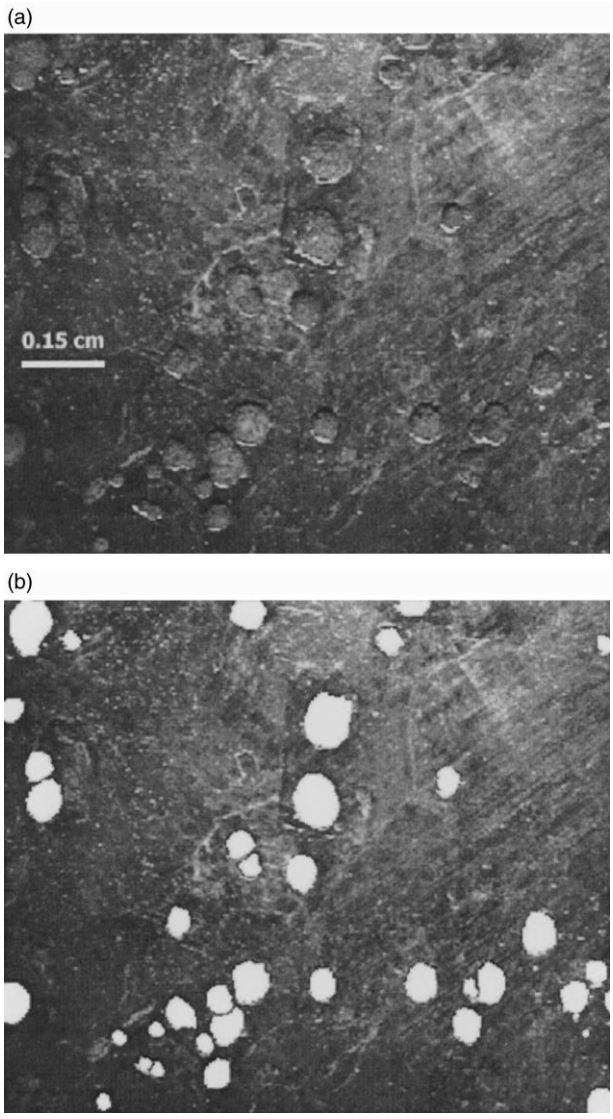

Fig. 1. Optical micrographs of part of the corroded face of sample Type 3, after removal of corrosion products: (a) as observed under the microscope, (b) after painting each pit using an image editor computer program.

3. Results and discussion

3.1. Characterisation of sputtered films

The thickness of the films, measured by scanning electron microscopy observation of the cross-section, is shown in Table 1 and was approximately equal to 3.5 μm in all cases with the exception of Type 5 coating due to the double deposition time. The slightly greater thickness of Type 3 coating (3.8 μm) can be attributed to the higher sputtering rate of W–Ti compared to W–Ti–N, and the lower thickness of Type 4 sample (3.2 μm) to the ion bombardment carried out during the interruption between deposition of the two layers.

Electron probe microanalysis (EPMA) was used to determine the chemical composition of the films and they were found to be very similar. A typical composition was: W 31, Ti 23, N 46 at%. The only exception to this was the Type 3 sample with a lower N content (37 at%), the reason being that the EPMA analysis depth is greater than the thickness of the W–Ti–N layer, reaching the W–Ti interlayer which does not contain N.

Fig. 2. Optical micrographs of one of the corroded faces of sample Type 3 after removal of the corrosion products.

3.2. General observations on corroded samples

Several deductions can be made concerning the corrosion of the various samples. The distribution of pits on the corroded surfaces is not uniform under these experimental conditions, as can be seen in Fig. 2, which shows the pits after corrosion products have been removed from the surface of the coating. This non-uniform distribution is similar to that obtained electrochemically in previous studies [1–3]. Additionally, there appear to be preferential zones for pit formation following the trajectories of vertical saline solution movement and of corrosion products, as demonstrated in Fig. 3.

The structure of the corrosion products on different zones of the film surface was identified by X-ray diffraction. No significant differences in the diffraction spectra were detected between the samples. Corrosion products on the surface, see Fig. 3 for an example, were orange-coloured and identified as lepidocrocite (γ-FeOOH) and akageneite (β-FeOOH). Akageneite is usually observed in the corrosion of steel in marine environments where it is a final product resulting from the oxidation of hydrated iron chloride [12] (also identified). Diffraction peaks corresponding to NaCl are also seen. The zone near the pits contains lepidocrocite and goethite (α-FeOOH) as well as signs of magnetite, Fe_3O_4, whereas zones with no observable corrosion have only small amounts of lepidocrocite. No tungsten or titanium oxides were detected.

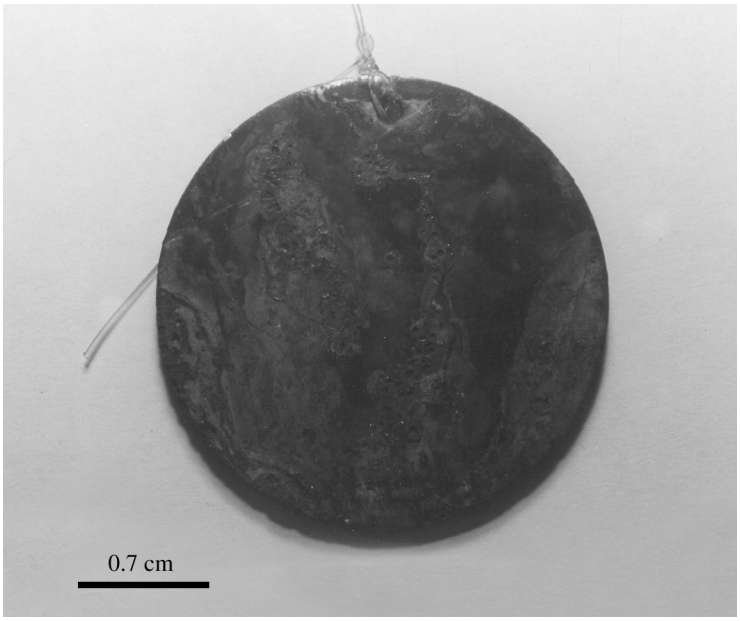

Fig. 3. Optical micrographs of one of the corroded faces of sample Type 2 immediately after removal from the salt spray test chamber.

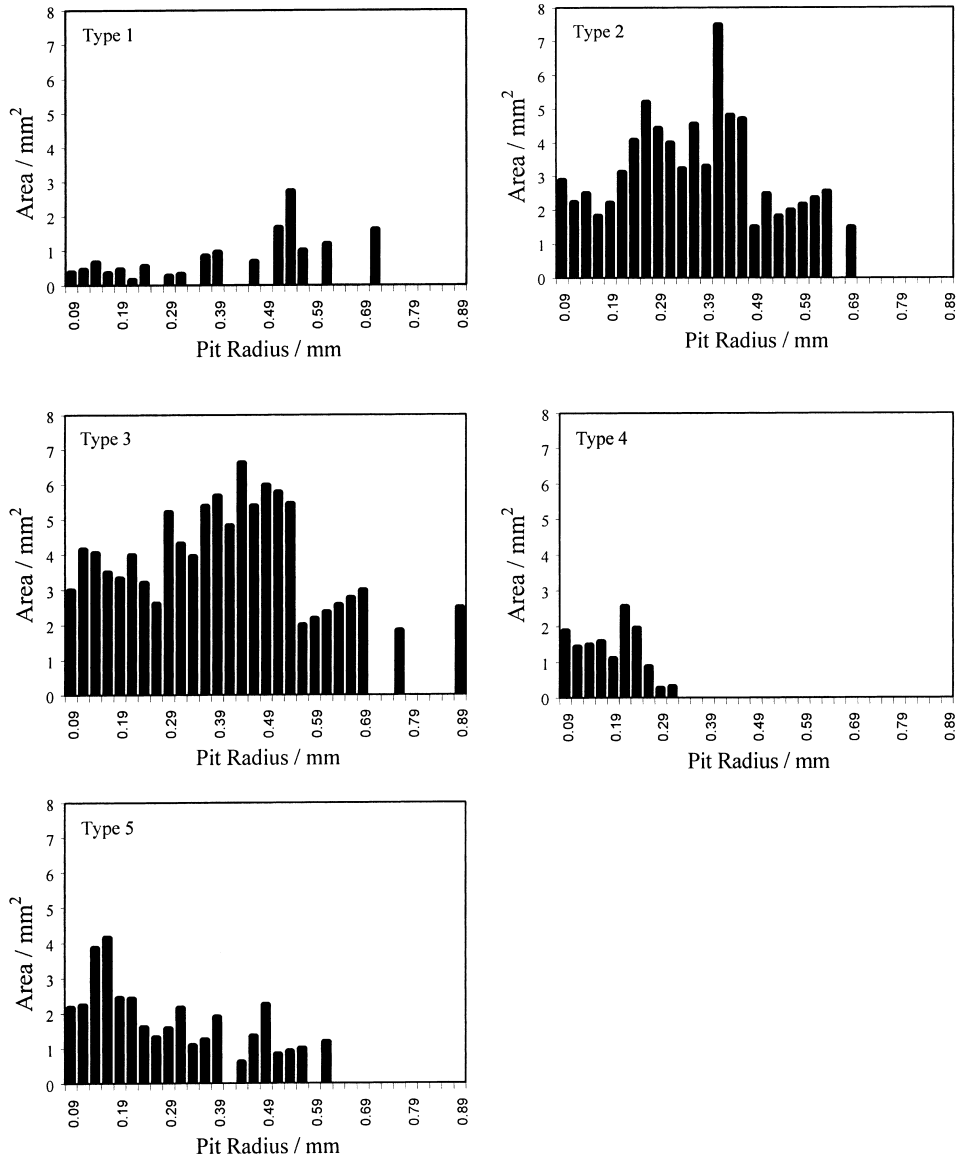

Fig. 4. Image analysis results for all types of sample shown as total pitted area as a function of pit radius.

3.3. Image analysis

All samples were treated by image analysis following the procedure described in Section 2. In Fig. 4 are shown results for the corroded samples, in terms of pit geometric area as a function of pit radius. Each of the bars corresponds to a range of pit radii of 0.025 mm. The surface shape of the pits is approximately circular and the vertical cross-sectional shape can be approximated as semi-elliptical with a ratio of depth-to-width of around 0.4, as checked with a profilometer. It is also a reasonable approximation that the actual internal surface area of the pit is proportional to the geometric pit area as seen from above and that pit radius and pit depth are also proportional. Obviously, the number of small pits is much higher than that of large pits but the contribution to the total corroded area is small.

Fig. 5 shows the variation of corroded area as a function of pit radius in normalized form. Table 2 gives further information concerning the image analysis of the sample surfaces after corrosion (see procedure in Section 2), as well as from visual inspection of the corroded samples when removed from the corrosion chamber. The visually-apparent extent of the surface degradation does not correspond to the effective area that was actually corroded.

Pertinent general observations are:

- Preferentially corroded zones, for all sample types, follow the lines of fluid

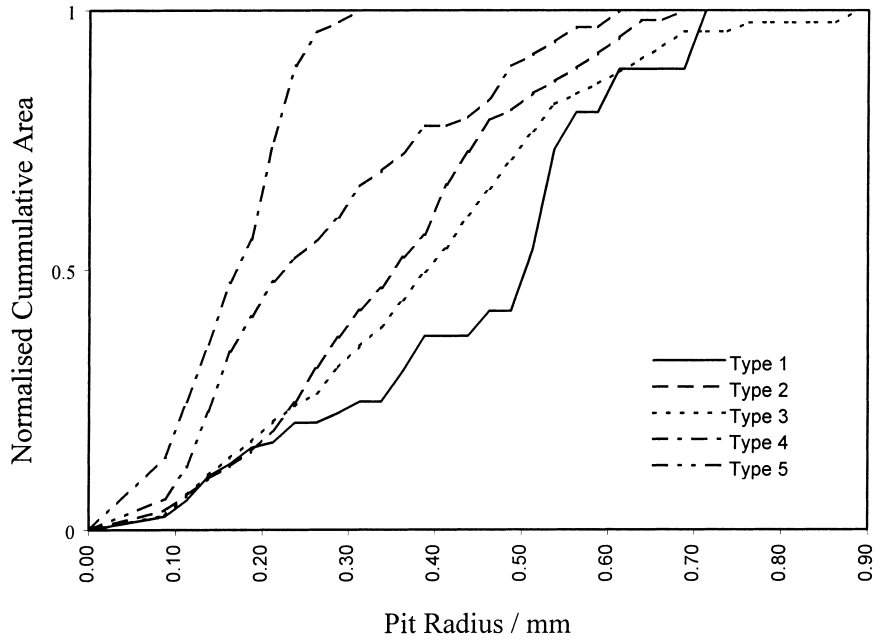

Fig. 5. Cumulative plots of corroded area; data from Fig. 4.

movement down the sample surfaces, and are where corrosion products accumulate, as demonstrated in Figs. 2 and 3.
- There is no clear correlation between the number and the total area of corrosion pits; only in sample Type 5 this correspondence exist approximately;
- One of the two faces of the sample is always more corroded than the other for all sample types; however, there is no correlation between the more corroded face and any particular positioning in the test chamber;

A number of deductions can be made:

- Type 1 has the best corrosion resistance with the lowest number and smallest area of corrosion pits;
- Sample Type 2 has a much higher number of corrosion pits than Type 1, but the corrosion process appears to be equally advanced for both, see Fig. 5. This can be attributed to its greater roughness with consequent easier penetration of electrolyte and accumulation of corrosion products on its surface, these being associated with preferential zones for pit formation. The same appears to happen for sputtered TiN films on carbon tool steel substrates [13].
- Type 4 has a very large number of tiny corrosion pits, clearly shown from the cumulative curve in Fig. 5, evidently different for all the other samples. This must be a reflection of the duplex film. Direct electrolyte penetration can only occur through sub-microscopic channels which are aligned between the two layers. The consequence is smaller pits.
- The major contribution to the total corroded area in sample Type 5 is also from small pits, the inverse of that observed for Type 1, see Fig. 5. Indeed, it has the smallest area covered with corrosion products (less than Type 1 and even Type 4 that only underwent the corrosion test during 3 days); however, the number and total area of corrosion pits are much higher than for Types 1 and 4. This reflects the influence of film thickness;
- Comparison of sample Types 2 and 3, which show a similar variation in

Table 2
Results from pitting corrosion in salt spray test

	Image analysis						Visual inspection: area of worse face corroded (%)	
	Face 1		Face 2		Total			
	N° pits	% area	N° pits	% area	N° pits	% area	After 3 days	After 5 days
Type 1	42	1.8	22	0.2	64	1.0	5	50
Type 2	142	6.4	289	4.4	431	5.4	traces	80
Type 3	259	9.3	300	5.5	559	7.4	5	70
Type 4	203	1.8	–	–	203	0.9	70	–[a]
Type 5	241	3.8	107	1.2	348	2.5	traces	30

[a] Sample removed after 3 days.

corroded area with pit radius, confirms that it is the stage to which the corrosion process has reached that determines the corrosion pit area. In both cases, the faces with smaller corroded areas have a higher number of corrosion pits, see Table 2, probably due to the fact that the extensive spalling or coating explosion did not yet occur. This will be further discussed below.

A similar plot to those in [11], of spot density vs. corroded area ratio, is shown in Fig. 6. The number of pits is proportional to the spot density in [11] since all samples had the same area. All the points for the five Types of sample fall in a band which moves diagonally upwards and to the right, in the same way as observed in [11], even including Type 4, which was removed after 3 days exposure.

3.4. Corrosion mechanism

In the light of these results, the model for the mechanism of corrosion explaining the formation of corrosion pits in W–Ti–N coated HSS steel substrate previously proposed [3] can be discussed in further detail.

The first step in the corrosion process corresponds to penetration of electrolyte ions through the substrate via irregularities or defects in the coating, the extent of penetration depending on the number of such defects. Thus, the best corrosion

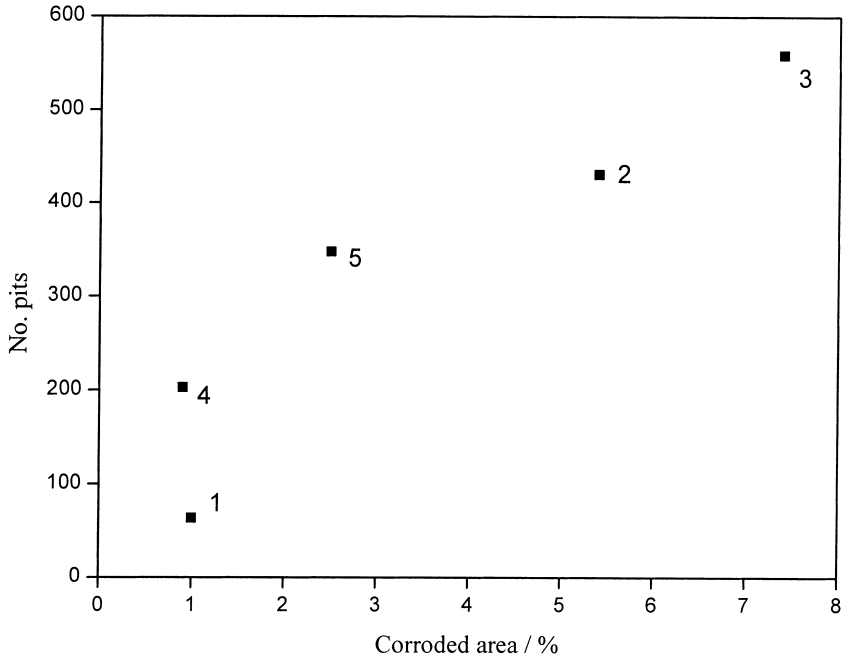

Fig. 6. Plot of number of pits vs. corroded area for the five sample types; data from Table 2.

resistance is that of Type 1, since it has the lowest number of defects in the coating, as shown by its very compact cross-section morphology, Fig. 7a, and the smoothest surface.

All the other samples have rougher surfaces and more open cross-section morphologies, Fig. 7b–e.

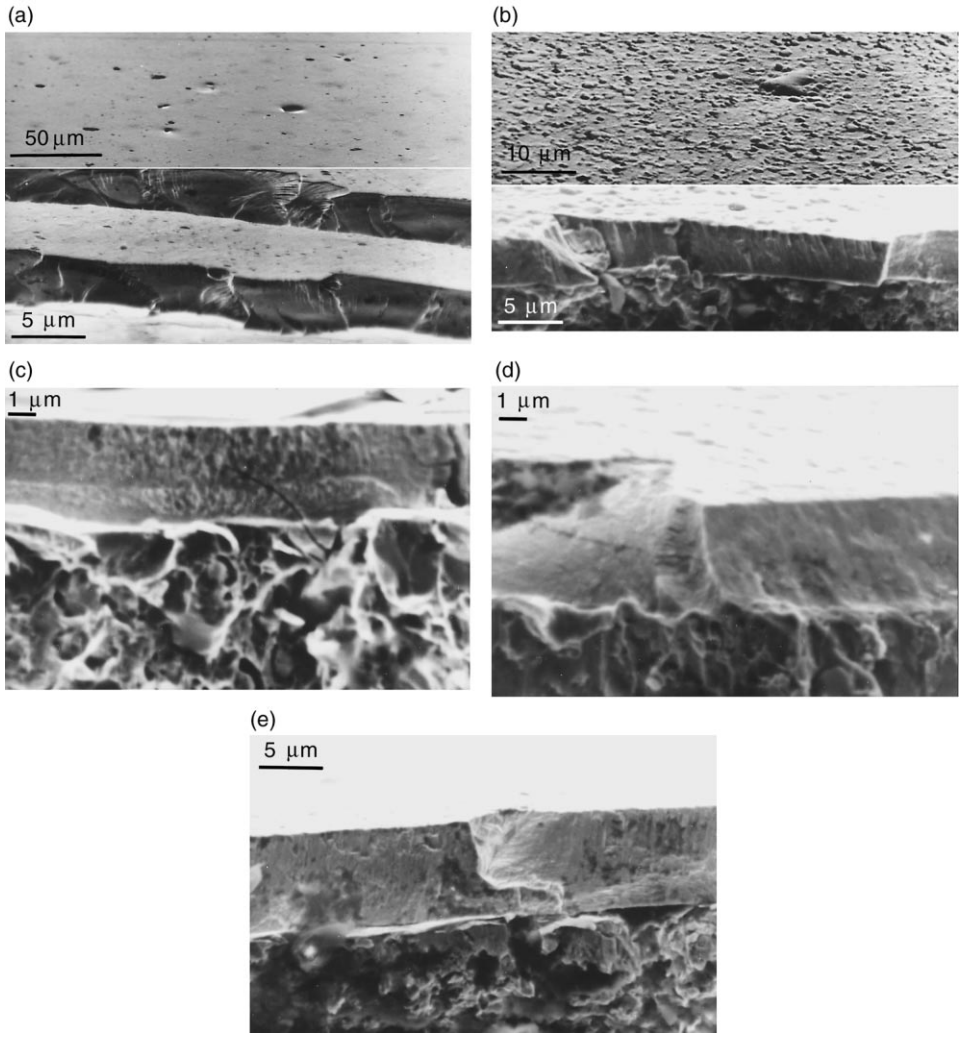

Fig. 7. SEM micrographs of the cross-section of the as-deposited W–Ti–N films (in (a) and (b) the upper part of the figure also shows the surface morphology of the sample): (a) Type 1 (b) Type 2 (c) Type 3 (d) Type 4 (e) Type 5.

- Type 2. The substrate surface was ion-bombarded during a longer time than sample Type 1. The higher substrate surface roughness obtained is maintained, and sometimes increased, during film deposition.
- Type 3 was a duplex film, the first layer being W–Ti (without N), which influences the cross-section morphology of the W–Ti–N film deposited on top of it. It is well known that the addition of N to metal-sputtered films leads to an increase in the density of the cross-section morphologies of the films [14]. However, close to the interface with the W–Ti layer this film will have a type T [15] morphology equal to that of W–Ti, which does not totally disappear by the outer surface of the W–Ti–N layer. This lower compactness permits easier electrolyte penetration.
- Type 4. The second etching enhances the irregularities in the coating surface leading to rougher samples and therefore, less compact morphology.
- Type 5. An increase in thickness leads to an increase of the growth of defects in sputtered films [16], with a higher number of pores near the surface in comparison to the film/substrate interface.

The second step corresponds to the corrosion processes occurring after electrolyte penetration. The substrate begins to corrode by pitting, forming mainly iron oxides/hydroxides (lepidocrocite, akagenite and goethite [17]) which accumulate at the interface between the coating and the substrate. Consequently, the corrosion products push the coating away from the substrate, leaving a protuberance over the corrosion pit, Fig. 8a. The accumulation of corrosion products constitutes a barrier to electrolyte penetration and retards further corrosion. This should occur in the early part of pit formation. Its duration depends on the capacity of the coating to support the growth of the protuberance without promoting extensive spalling of the coating. A greater coating thickness will improve the mechanical stability of the protuberance owing to the superior lateral support that it provides, which can explain the lowest accumulation of corrosion products on the surface of sample Type 5, and the lower number and lower total area of corrosion pits compared to Types 2 and 3. For many corrosion sites, blocking of the penetration channels will be irreversible and corrosion will cease, equivalent to pit death. For others, blocking will not occur so that the coating will be partly, Fig. 8a, or totally, Fig. 8b, removed.

However, in some cases, the accumulation of corrosion products under the coating together with a high degree of blocking creates such a high pressure that the coating explodes, as seen previously [3], leaving the corrosion pit uncovered and with a concentric ring of corrosion products on the uncorroded film surface. This will be favoured in situations where the protuberance reaches a sufficiently high aspect ratio. Following rupture, corrosion will proceed very fast, giving rise to deep and large pits, Fig. 8c and d, occasionally with some film removal next to the pit itself, Fig. 8e. However, in the major part of the pit perimeter, the W–Ti–N coating remains attached to the substrate, Fig. 8f.

Finally, it should also be remembered that the formation of corrosion pits will depend on the local microscopic environment. The ease of accumulation of

corrosion products on a vertically-oriented sample must be related to surface roughness, which can aid in retaining the electrolyte, which would otherwise flow downwards. Thus, the higher the surface roughness, the more pit formation is favoured.

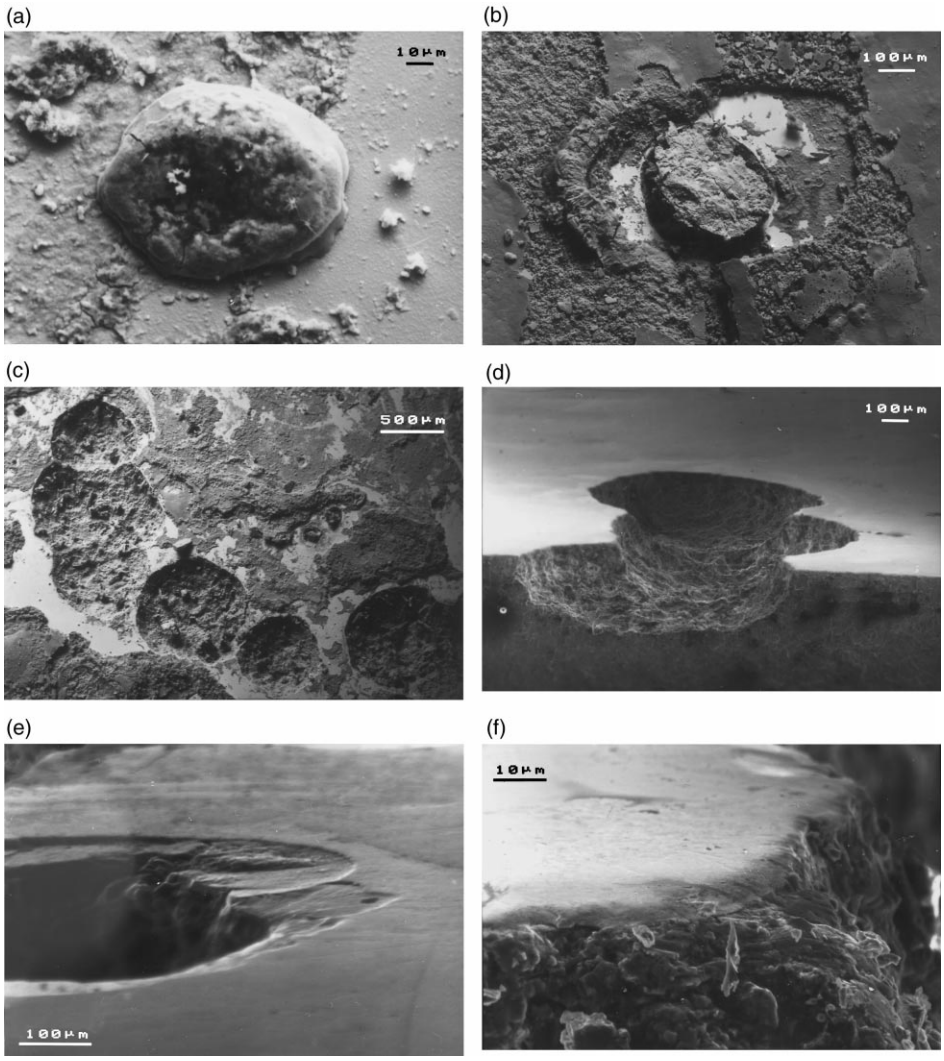

Fig. 8. SEM micrographs of corroded W–Ti–N coated samples. (a) Protuberance formed during the corrosion process without spalling. (b) A later state of the corrosion process at which no film remains, but without coating rupture by explosion. (c) Open corrosion pits. (d) Open corrosion pits in cross-section view. (e) Detail of an open corrosion pit showing coating delamination induced by pit explosion. (f) Detail of a corrosion pit showing the W–Ti–N film adherent to the substrate at the pit edge.

4. Conclusion

This work has examined the corrosion of W–Ti–N coatings made under different deposition conditions, using the salt spray test and, principally, image analysis to examine the size and distribution of the corrosion pits formed. It is seen that image analysis is a valuable technique for analysing the pitting data obtained and comparing various types of sample films. Further applications in the future can be predicted.

Corrosion is determined by penetration of electrolyte through the substrate. Film morphology is the most important parameter in determining the rate of corrosion. Factors such as increased surface roughness, an underlayer and/or interrupted deposition have influence on the properties of the coating and on the corrosion behaviour. Compared to the usual procedure for coating preparation, increased surface roughness leads to a lower corrosion resistance; the main possible improvement arises from compactness and increased film thickness.

Acknowledgements

The authors thank Eng. F. Ramos, HUF Portuguesa, for carrying out the salt spray tests.

References

[1] C.M.A. Brett, A. Cavaleiro, Mat. Sci. Forum 192–194 (1995) 797.
[2] C.M.A. Brett, C.-M. Nimigean, Thin Solid Films 311 (1997) 1.
[3] C.M.A. Brett, A. Cavaleiro, Thin Solid Films 322 (1998) 263.
[4] A. Cavaleiro, C. Louro, J.V. Fernandes, C.M.A. Brett, Vacuum 52 (1999) 157.
[5] B. Normand, A. Pierre, J. Pagetti, Corros. Sci. 37 (1995) 1537.
[6] M. Janik-Czachor, M.B. Ives, in: R.P. Frankenthal, J. Kruger (Eds.), Passivity of Metals, The Electrochem. Soc., Princeton, NJ, 1978, p. 369.
[7] M. Janik-Czachor, J. Electrochem. Soc. 128 (1981) 513C.
[8] T. Shibata, T. Takeyama, Corrosion 33 (1977) 243.
[9] D.E. Williams, C. Westcott, M. Fleischmann, J. Electrochem. Soc. 132 (1985) 1796.
[10] D.E. Williams, C. Westcott, M. Fleischmann, J. Electrochem. Soc. 132 (1985) 1804.
[11] I. Muto, H. Kihira, Mater. Sci. Forum 185-188 (1995) 1057.
[12] B.S. Skerry, J.B. Johnston, G.C. Wood, Corros. Sci. 28 (1988) 657.
[13] J. Munemasa, T. Kumakiri, Surf. Coat. Technol. 49 (1991) 496.
[14] A.G. Dirks, R.A.M. Wolters, A.E.M. de Veirman, Thin Solid Films 208 (1992) 181.
[15] J.A. Thornton, J. Vac. Sci. Technol. A 4 (1986) 3059.
[16] R. Messier, A.P. Giri, R.A. Roy, J. Vac. Sci. Technol. A 2 (1984) 500.
[17] A. Cavaleiro, C.M.A. Brett, in: L. Faria (Ed.), Proceedings of EUROMAT'98, Sociedade Portuguesa dos Materiais, Lisbon, 1998, p. 233.